EurJIC
European Journal of Inorganic Chemistry

Research Article
doi.org/10.1002/ejic.202200322

Chemistry Europe
European Chemical Societies Publishing

www.eurjic.org

Thermal Structure Transformation of Methylammonium Vanadate and it's Application as a Negative Staining Reagent for Observing SARS-CoV-2

Ndaru Candra Sukmana,[a] Sugiarto,[a] Jun Shinogi,[a] Akima Yamamoto,[b] Akifumi Higashiura,[b] Takemasa Sakaguchi,[b] and Masahiro Sadakane*[a]

The solid-state thermal structure transformation of methylammonium vanadate, $(CH_3NH_3)VO_3$, from −150 °C to 350 °C is reported. Variable-temperature X-ray single-crystal structure analysis at 23, 0, −50, −100, and −150 °C reveal $(CH_3NH_3)VO_3$ comprises of methylammonium cations and "snake-like" $([VO_3]^-)_n$ anion chains propagating along the *c*-direction in the $Pna2_1$ space group. In between −150 and −100 °C, we observe a reversible structural transformation due to the re-orientation of the methylammonium cations in the crystal packing, which is also confirmed by the reversible profiles observed in differential scanning calorimetry. The methylammonium vanadate is stable until at ca. 100 °C and further heating releases methylamine and water and V_2O_5 is formed at ca. 275 °C . Furthermore, we show that the methylammonium vanadate can be used as a negative staining reagent for visualizing SARS-CoV-2, allowing us to discern the spike proteins from the body of the virus using transmission electron microscopy.

Introduction

Polyoxometalates are a large family of polynuclear oxo–hydroxo complexes of early transition metals (tungsten, molybdenum, vanadium, or niobium).[1] Polyoxometalates form a wide variety of compositions and structures that produce different physical and chemical properties, such as negative charges, oxo-enriched surfaces, acid-base properties, and redox potential.[1–3] These properties have led to their wide use as the main compounds in catalysts,[4,5] electrocatalysts,[6,7] medicines,[8] sensors,[9] and staining reagents.[10,11] Normally, polyoxometalates are synthesized via the condensation of oxoanions (MoO_4^{2-}, WO_4^{2-}, or VO_4^{3-}) using a self-assembly process.[1,12] The formation of polyoxometalates is influenced by experimental conditions, such as the type and concentration of component metals and counter-cations, temperature, solvent, and pH of the solution.[12,13]

Polyoxovanadates, a subclass of polyoxometalates, are unique polyoxometalates due to the variable oxidation state of vanadium (+3, +4, and +5) and the coordination spheres of V–O polyhedra (VO_4 tetrahedron, VO_5 square pyramid and trigonal bipyramid, and VO_6 octahedron).[12,14–16] Previous studies have reported several polyoxovanadates that may contain either fully oxidized, reduced, or mixed-valence vanadium species, such as $[V_2O_7]^{4-}$,[17] $[V_3O_9]^{3-}$,[18] $[V_4O_{12}]^{4-}$,[19] $[V_5O_{14}]^{3-}$,[20] $[V_{10}O_{28}]^{6-}$,[21] $[V_{12}O_{32}]^{4-}$,[22] $[V_{13}O_{34}]^{3-}$,[22] $[V_{15}O_{36}]^{5-}$,[23] $[H_4V_{15}O_{42}]^{5-}$,[24] $[V_{16}O_{42}]^{4-}$,[25] $[V_{17}O_{42}]^{4-}$,[26] $[V_{18}O_{42}(PO_4)]^{11-}$,[27] $[V_{19}O_{41}(OH)_9]^{8-}$,[28] $[V_{34}O_{82}]^{10-}$,[29] and polymeric $([VO_3]^-)_\infty$.[30,31] In general, polyoxovanadates have a wide range of applications in medicine,[32] bioinorganic chemistry,[33] homogeneous and heterogeneous catalysis,[34] and as staining reagents.[35]

Herein, we report that methylammonium vanadate $(CH_3NH_3)VO_3$,[30] which has been used as a staining reagent,[35] exhibits a reversible structural transformation by switching the direction of the methylammonium molecules in the temperature range of −150 to −100 °C. In contrast, heating at ~275 °C irreversibly releases methylamine and water to form V_2O_5. Although the room temperature (at 23 °C) structure of methylammonium vanadate, which has a "snake-like" chain motive (Figure 1), is known,[30] the thermally-induced reversible rearrangement of methylammonium cations in the crystal packing,

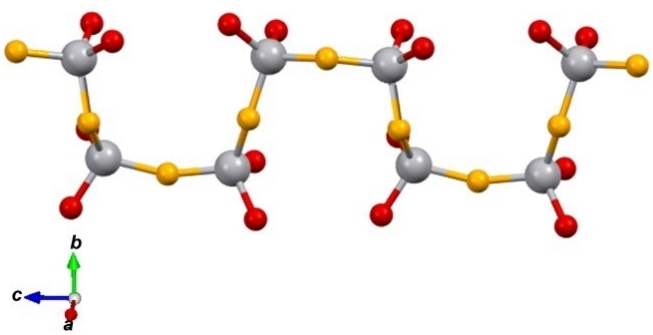

Figure 1. "Snake-like" chain structure of a $([VO_3]^-)_n$ anion along the *c*-direction. Grey, red, and yellow balls represent vanadium, terminal oxygen, and bridging oxygen, respectively.

[a] N. C. Sukmana, Sugiarto, J. Shinogi, Prof. M. Sadakane
Department of Applied Chemistry, Graduate School of Engineering, Hiroshima University
1-4-1 Higashihiroshima, Kagamiyama, 739-8527 Higashi-Hiroshima, Japan
E-mail: sadakane09@hiroshima-u.ac.jp
home.hiroshima-u.ac.jp/catalche
[b] A. Yamamoto, A. Higashiura, T. Sakaguchi
Department of Virology, Graduate School of Biomedical and Health Sciences, Hiroshima University
1-2-3 Kasumi, Minami-ku, 734-8551 Hiroshima, Japan

Supporting information for this article is available on the WWW under https://doi.org/10.1002/ejic.202200322

Research Article
doi.org/10.1002/ejic.202200322

however, has not been reported to date. The motion of methylammonium cations in crystal packing is gaining increasing interest in the field of lead halide perovskites because it affects the optical and electronic properties of solids.[36,37]

Polyoxovanadates have been used as bioinorganic drugs due to their ability to interact with proteins, affecting various biological processes.[32,38–40] In the present work, we also report that the methylammonium vanadate can be used as a staining reagent for visualizing coronaviruses using transmission electron microscopy. Coronaviruses cause severe respiratory diseases: severe acute respiratory syndrome (SARS) and Middle East respiratory syndrome (MERS). It is a highly pathogenic virus that has rapidly spread worldwide.[41] The enveloped virus, SARS-CoV-2, is responsible for the COVID-19 pandemic.[42]

Electron microscopic visualization of negatively stained SARS-CoV-2 is a valuable technique for viewing the detailed morphology and size of the intact virus. Heavy metal negative staining is a well-established technique for contrasting thin biological materials and is frequently used in diagnostic microscopy.[43] Among the various polyoxometalates used as negative staining reagents, methylamine-containing vanadate is known to be a negative staining reagent.[35] However, the detailed preparation method and structure of the commercially available "methylamine vanadate" negative staining reagent have not been reported.

Results and Discussion

Synthesis and variable-temperature single-crystal structure analysis

Methylammonium vanadate was prepared upon dissolving V_2O_5 in methylamine solution (40%) with a methylamine/vanadium ratio of 2.8 at room temperature and subsequent drying at 70 °C. Colorless crystals suitable for single-crystal X-ray structure analysis were obtained via recrystallization of the crude solid from water.

Single crystal X-ray diffraction analysis at 23 and −150 °C demonstrated that an asymmetric unit contains four methylammonium cations and a "snake-like" $([VO_3]_4)^{4-}$ anion chain along the *c*-direction in the $Pna2_1$ space group (Figure 1 and Figure 2, and Table 1 and S1). The $CH_3NH_3^+$ cations were located between the parallel chains. All of the V atoms in the $([VO_3]_4)^{4-}$ anion have a distorted tetrahedral $[VO_4]$ geometry. There are two types of oxygen in the structure: Terminal oxygens (O1, O2, O5, O6, O8, O9, O11, and O12) and bridging oxygens between two V atoms (O3, O4, O7, and O10). Tetrahedral $[VO_4]$ connected via corner-sharing bridging atoms form infinite chains.

The crystal structure obtained at 23 °C was the same as the one reported by Averbuch-Pouchot and Durif,[30] which is different from the reported straight-chain structure of ammonium metavanadate, $(NH_4)VO_3$.[31] The distance between

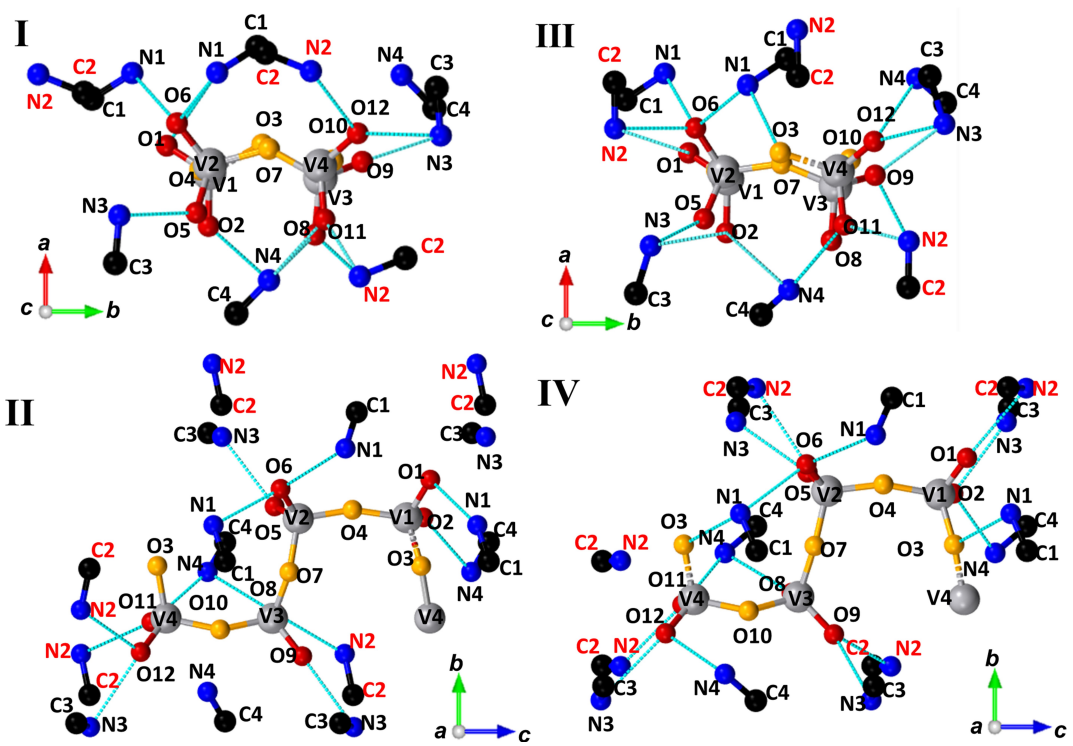

Figure 2. Crystal structure and atom labeling for methylammonium vanadate obtained at temperature 23 °C viewed along the *c*-direction (I) and *a*-direction (II), and at −150 °C viewed along the *c*-direction (III) and *a*-direction (IV). Hydrogen atoms were omitted for clarity. Grey, red, yellow, black, and blue balls represent vanadium, terminal oxygen, bridging oxygen, carbon, and nitrogen atoms, respectively. Light blue lines represent the hydrogen bonds formed between the N and O atom, which are shorter than 3.0 Å.

Research Article
doi.org/10.1002/ejic.202200322

Table 1. Crystal data obtained for methylammonium vanadate.

Empirical formula	CNH_6VO_3 (**1**)	CNH_6VO_3 (**2**)
Formula weight [g/mol]	131	131
Temperature	23 °C (296 K)	−150 °C (123 K)
Crystal system	Orthorhombic	Orthorhombic
Space group	$Pna2_1$	$Pna2_1$
a (Å)	11.9092(11)	12.5397(8)
b (Å)	18.6442(17)	17.4526(11)
c (Å)	8.4751(8)	8.4880(5)
α (°)	90	90
β (°)	90	90
γ (°)	90	90
V (Å^3)	1881.8(3)	1857.6(2)
Z	16	16
$D_{calcd.}$ [g/cm^{-3}]	1.850	1.874
μ [mm^{-1}]	1.983	2.009
Radiation	Mo Kα (λ = 0.71073 Å)	Mo Kα (λ = 0.71073 Å)
F(000)	1056.0	1056.0
G.O.F.	1.061	1.037
R indexes [$I > 2\sigma(I)$]	$R_1 = 0.0276$; $wR_2 = 0.0702$	$R_1 = 0.0222$; $wR_2 = 0.0529$
R indexes [all data]	$R_1 = 0.0310$; $wR_2 = 0.0724$	$R_1 = 0.0242$; $wR_2 = 0.0540$

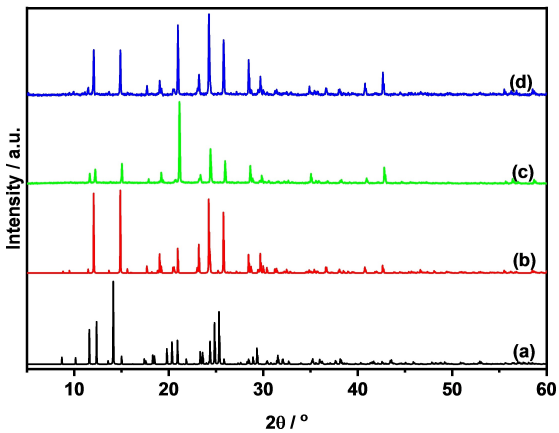

Figure 3. Simulated XRD patterns for methylammonium vanadate based on the single-crystal data measured at −150 °C (a) and 23 °C (b), and the XRD patterns observed for methylammonium vanadate after evaporation (c) and being heated at 100 °C (d).

the vanadium and terminal oxygen atoms has an average value of 1.64 Å, and that between vanadium and the bridging oxygen atoms was 1.79 Å. The O–V–O angle varies from 106.96° to 112.21°. Selected bond lengths and angles are listed in Table S2 and S3, respectively. The bond valence sum (BVS) indicated that vanadium was in the +5 oxidation state (Table S4). Elemental analysis indicates that the formula is $CH_3NH_3[VO_3]$, and ^{51}V NMR of the methylammonium vanadate could be measured (see below) which also confirm the vanadium was in the 5+ oxidation state.

Decreasing the analysis temperature to −150 °C caused an increase in the *a*-axis (~5%) and a decrease in the *b*-axis (~6%) and left the *c*-axis remained unchanged. The cell volumes were decreased at −150 °C (~1%). A "snake-like" chain along the *c*-direction was still observed. The simulated diffraction pattern obtained using the single-crystal X-ray data of the crystal at −150 °C was different from the crystal at 23 °C (Figure 3 (a) and (b)), indicating that a single-crystal to single-crystal transformation occurred. The distance between the vanadium and terminal oxygen atoms has an average value of 1.65 Å and the distance between the vanadium and bridging oxygen atoms was 1.80 Å. The O–V–O angle varies from 106.29° to 112.30°. Selected bond lengths and angles are listed in Tables S2 and S3, respectively. The BVS results indicated that vanadium was in the 5+ oxidation state (Table S5).

One major difference between the crystals observed at 23 and −150 °C was the position of one ($C2H_3$–$N2H_3^+$) methylammonium cation. The methylammonium cation ($C2H_3$–$N2H_3^+$) in the crystal at −150 °C was parallel to the *a*-axis. However, the same methylammonium cation was parallel to the *b*-axis in the crystal observed at 23 °C (Figure 2). The orientation of this cation causes different interactions with the vanadate anions. Hydrogen bonds play a crucial role in crystal formation because the terminal and bridging oxygen atoms can act as donors to generate hydrogen bonds with nearby $CH_3NH_3^+$ cations. Figure 2 shows the hydrogen bonds between the N and O atoms with a distance of < 3 Å and Table S6 shows the hydrogen bond lengths between the N and O atoms.

Figure 2 and Figure S1 show four methylammonium molecules in the crystal at 23 and −150 °C. The first methylammonium (C1–N1) in the crystal observed at 23 °C interacts with two terminal oxygen atoms in the same chain (O6, O1) and one terminal oxygen atom of another chain (O6); C1–N1 in the crystal observed at −150 °C, in contrast, was connected to the terminal and bridging oxygen atoms in the same chain (O6, O3) and one terminal oxygen atom of another chain (O6). The second methylammonium (C2–N2) in the crystal observed at 23 °C interacts with two terminal oxygen atoms in the same chain (O8, O11) and one terminal oxygen from another chain (O12); C2–N2 in the crystal observed at −150 °C, in contrast, was connected to each of the two oxygen terminals of the two chains (O9, O11, O1, O6). The third methylammonium (C3–N3) in the crystal observed at 23 °C interacts with two terminal oxygen atoms of the same chain (O9, O12) and one terminal oxygen from another chain (O5); C3–N3 in the crystal observed at −150 °C, in contrast, was connected to two terminal oxygen atoms of the same chain (O5, O2) and two terminal oxygen from another chain (O9, O12). The last methylammonium (C4–N4) in the crystal at 23 °C interacts with three terminal oxygen atoms of the same chain (O2, O8, O11); C4–N4 in the crystal at −150 °C, in contrast, was connected to three terminal oxygen atoms of the same chain (O2, O8, O11) and one terminal oxygen from another chain (O12). Based on these results, the crystal structure observed at −150 °C contains more hydrogen bonds. These make the structure denser and therefore, the cell volume of the crystal observed at −150 °C (1857.6 Å^3) was lower than at 23 °C (1881.8 Å^3).

Single-crystal X-ray structural analyses were performed at different temperatures (Figure 4 and Table S1). When the temperature was decreased from 23 °C, all of the axis lengths were slightly decreased till −100 °C. In contrast, cooling at −150 °C suddenly increases the *a*-axis length and decreased *b*-

Research Article
doi.org/10.1002/ejic.202200322

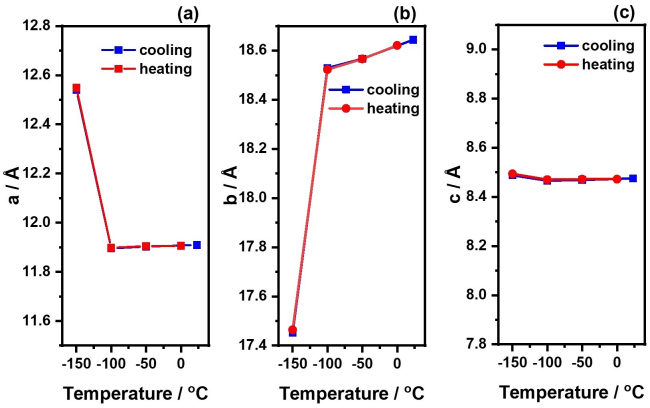

Figure 4. Unit cell parameters of methylammonium vanadate upon cooling and heating. *a*-axis (a), *b*-axis (b), and *c*-axis (c).

axis lengths, indicating that the crystal structure changed between −100 and −150 °C. On the other hand, heating from −150 to −100 °C decreased the *a*-axis length and increased *b*-axis lengths. The unit cell parameters of the crystals changed during cooling and heating were fully reversible when the temperature exceeded the transformation temperature during either cooling or heating.

DSC measurements were carried out in cooling and heating mode (10 °C min^{-1}) in the temperature range of 25 to −147 °C under a flow of nitrogen gas (Figure 5). The DSC thermogram shows the reversibility of the phase transformation between the two crystals. An exothermic peak was observed at −119 °C (536 J mol^{-1}) upon cooling and an endothermic peak was observed at −103 °C (677 J mol^{-1}) upon heating with a thermal hysteresis of approximately 16 °C, which is a typical of single-crystal-to-single-crystal systems.[44,45] This result was in agreement with the results of our single-crystal X-ray diffraction study, in which the crystal structure was reversibly transformed between −100 and −150 °C.

Characterization of methylammonium vanadate

The simulated and experimental powder XRD patterns obtained for methylammonium vanadate are shown in Figure 3. Peak positions of the experimental powder XRD profiles obtained after heating at 70 and 100 °C were similar to the simulated powder XRD pattern obtained using the single-crystal X-ray data at 23 °C. This result indicates that the powder had the same crystal structure, and the phase purity of the bulk powder was satisfactory.

Figure 6 shows the solid-state Raman spectra obtained for methylamine hydrochloride and methylammonium vanadate. The Raman band observed at 1004 cm^{-1} was attributed to the C–N stretching vibration of methylammonium, which confirmed the presence of methylammonium as a counter cation. Methylammonium vanadate exhibits a strong Raman band at 947 cm^{-1}, which can be attributed to the symmetric stretching of di-oxo $V(=O)_2$ unit.[46] Symmetric and asymmetric V–O bridging stretching modes were observed at 480 and 644 cm^{-1}, respectively. The Raman spectrum shows two features at 896 and 928 cm^{-1} (shoulder), which can be attributed to the asymmetric and symmetric V–O terminal stretching vibrations, respectively.[47]

The FT-IR spectrum of methylammonium vanadate contains bands assignable to $V=O_t$ at 939, 919, and 894 cm^{-1}; $V-O_b-V$ at 831, 777, and 655 cm^{-1}; and NH_3^+ and CH_3 bending at 1496, 1469, 1425, and 1265 cm^{-1} (Figure 7).[19,48]

In addition, the structure of methylammonium vanadate in water was checked by ^{51}V NMR. Figure 8 shows the ^{51}V NMR spectrum of methylammonium vanadate (0.5 wt.%) in H_2O which is used as negative staining reagent (see below). The major vanadate is tetravanadate $[V_4O_{12}]^{4-}$ (−587 ppm) together with pentavanadate $[V_5O_{15}]^{5-}$ (−584 ppm), divanadate $[V_2O_7]^{4-}$ (−572 ppm), and monovanadate $[VO_4]^{3-}$ (−560 ppm) which is similar to the case of $NaVO_3$.[49] Increase of the concentration increased amount of pentavanadate (Figure S2). It is known that several kind of vanadate species exist in equilibrium in solution.[50] The UV-Vis absorption spectrum of methylammonium vanadate in water (Figure S3) exhibits absorption

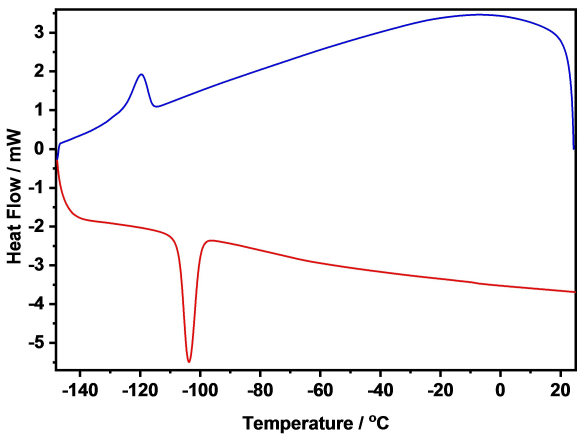

Figure 5. DSC curves obtained for methylammonium vanadate (10 °C min^{-1}) in cooling (blue line) and heating (red line) mode.

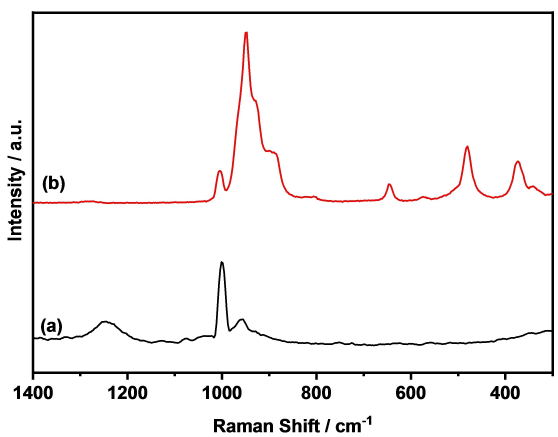

Figure 6. Raman spectra obtained for methylamine hydrochloride ($CH_3NH_3^+Cl^-$) (a) and methylammonium vanadate (b).

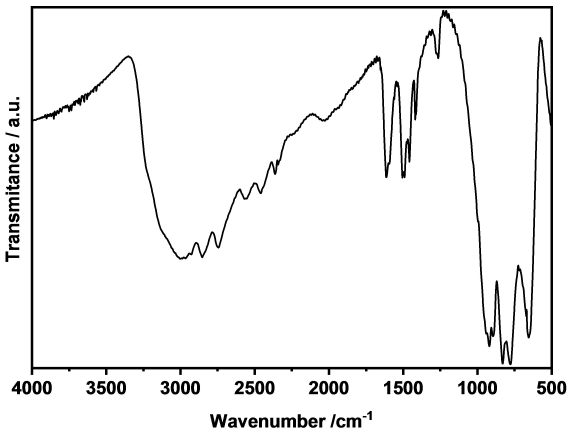

Figure 7. FT-IR spectrum obtained for methylammonium vanadate.

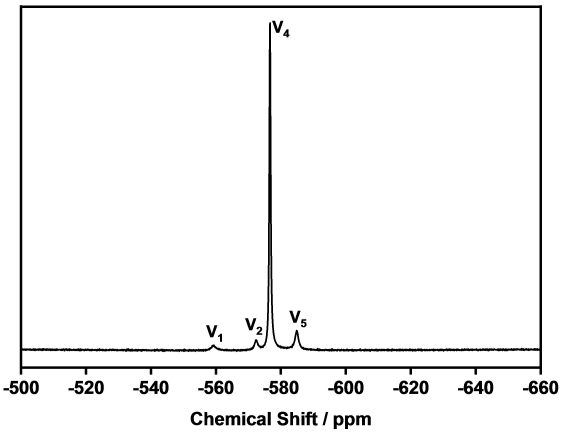

Figure 8. ^{51}V NMR spectrum of methylammonium vanadate in H_2O at concentration 38 mM (0.5 wt.%).

peaks centered at 207 and 266 nm, which can be attributed to the $O_t \rightarrow V$ and $O_b \rightarrow V$ charge transfer, respectively.[51]

Structural transformation during heating

The thermogravimetric (TG) and differential thermal analysis (DTA) curves obtained for methylammonium vanadate in air (Figure 9) show multistep weight loss. The results show that the compound was stable below 100 °C. Based on the TG curve, 30.6 % of weight loss occurred up to 400 °C. This weight loss corresponds to one methylammonium and 0.5 H_2O from $(CH_3NH_3)VO_3$ to form 0.5 V_2O_5 (30.5 %).

Temperature-programmed desorption-mass spectrometry (TPD-MS) under a flow of helium gas and TG-DTA under a flow of nitrogen gas were used to study the evolution of methylammonium upon heating (Figure 10). Several gases with *m/z* values of 44, 31, 30, 28, 18, 17, and 16 were also observed (Table S7). The first decomposition step was observed at < 200 °C, where the most methylammonium was eliminated. In addition to the desorption of H_2O and CH_3NH_2, the oxidation

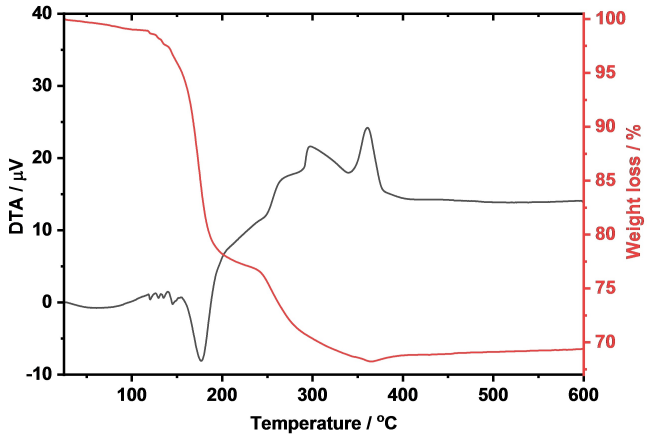

Figure 9. TG/DTA curves obtained for methylammonium vanadate under a flow of air.

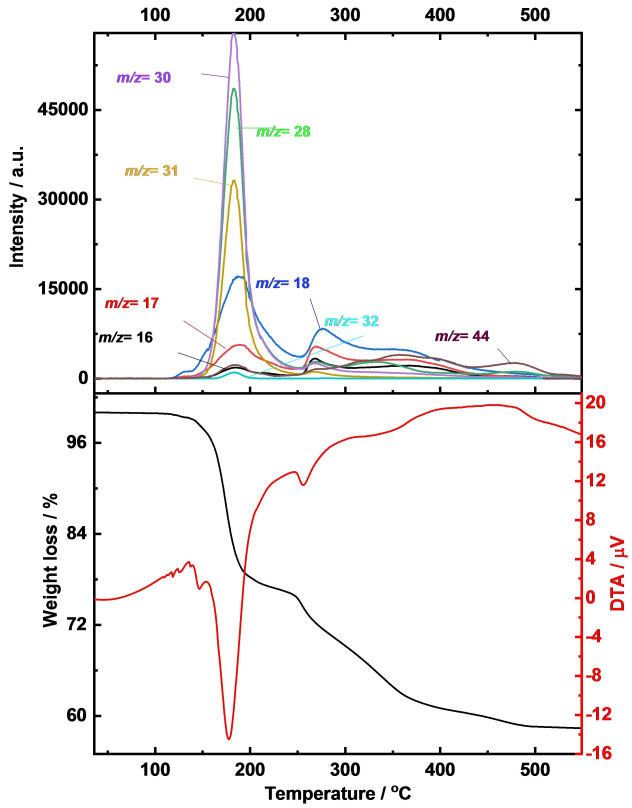

Figure 10. TG/DTA curves obtained under a flow of nitrogen gas and TPD-MS profile obtained under a flow of He gas for methylammonium vanadate.

and degradation products of methylammonium, such as NH_3, CO, N_2, NO, CO_2, and N_2O, were also observed, indicating the occurrence of a redox reaction between methylammonium and V=O. Similar degradation and oxidation reactions of methylamine in methylammonium paradodecatungstate have been reported.[52] The next decomposition step was observed upon further increasing the temperature.

Subsequently, we investigated the structural transformation of methylammonium vanadate during heating using infrared

Research Article
doi.org/10.1002/ejic.202200322

spectroscopy and X-ray powder diffraction. Upon heating, the intensity of the IR bands of methylammonium decreased, indicating that the counter-cations were gradually released and completely removed at $<200\,^{\circ}C$ (Figure S4). Figure S5 shows the powder XRD pattern of the heated methylammonium vanadate sample. The crystal structure was only stable up to 100 °C. The main peaks corresponding to methylammonium vanadate disappear after heating the solid at $>125\,^{\circ}C$. The release of methylammonium and water results in the formation of an amorphous compound. V_2O_5 was formed as the final product upon heating to 275 °C.

Application of methylammonium vanadate as a staining reagent

Methylamine metalate, which contains vanadate and tungstate, has been utilized as a staining reagent for virus observation using TEM.[35,53] We applied our prepared methylammonium vanadate to observe the SARS-CoV-2 Delta variant together with methylammonium tungstate for comparison. The staining methylammonium vanadate solution with a concentration of 0.5 wt.% in water were placed on the carbon film where the viruse have been adsorbed and the excess solution was removed using filter paper followed by drying before TEM observation. The TEM images reveal that both methylammonium vanadate and tungstate are suitable staining reagents for observing surface spike proteins and the images were consistent with those previously reported for coronaviruses (Figure 11 and Figure 12).[54] The most unique morphological feature of this virus is the presence of the characteristic crown-shaped viral surface spike protein, from which the name coronavirus is derived. In our research, the average diameter of the virus particles was 92 nm and the length of the spike was 18 nm, which were in agreement with those previously reported.[54]

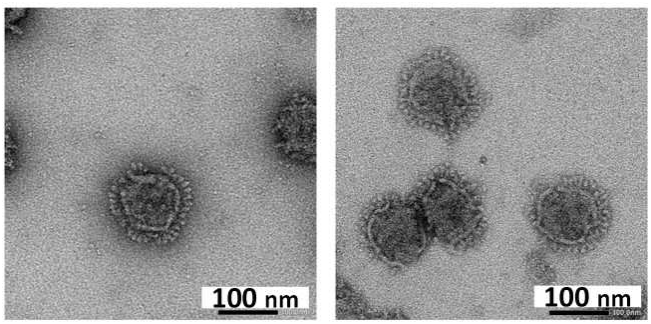

Figure 11. SARS-CoV-2 virions stained with 0.5 wt.% solution of methylammonium vanadate.

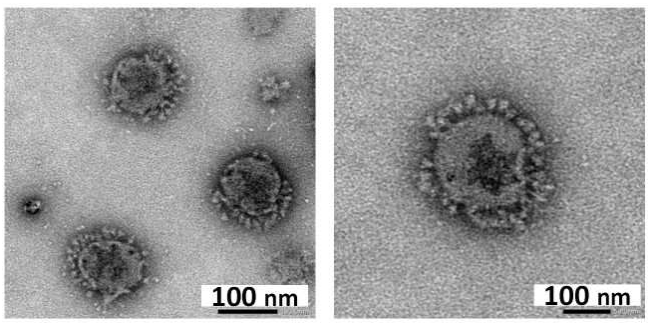

Figure 12. SARS-CoV-2 virions stained with 0.5 wt.% solution of methylammonium paradodecatungstate.

The ^{51}V NMR spectrum of the colorless staining solution (0.5 wt%, pH 6.9) shows that tetravanadate $[V_4O_{12}]^{4-}$ is the predominant species together with other V species (Figure 8). The existence of tetravanadate was further confirmed by Raman spectroscopy (Figure S6).[46] These polyoxovanadate species might interact proteins on virus and carbon film surface. Drying of the staining solution increases the concentration of vanadium and might produce more condensed species. Under the vacuum condition in TEM experiment, vanadate solids coats around viruses. Further investigation to understand vanadate species coating the viruses are underway in our group.

Conclusions

The solid-state reversible thermal structural transformation of methylammonium vanadate, $(CH_3NH_3)VO_3$, at ca. $-110\,^{\circ}C$ has been observed. Single-crystal X-ray structural analysis at different temperatures indicated that the structural transformation was due to a change in the direction of the methylammonium cation. However, heating causes decomposition to form V_2O_5. Furthermore, we have shown that methylammonium vanadate is a good negative staining reagent for coronaviruses using transmission electron microscopy (TEM).

Experimental Section

Materials: All chemicals were of reagent grade and used without further purification. V_2O_5 was purchased from Kojundo Chemical Laboratory Co., Ltd. and 40% methylamine solution was purchased from Kanto Chemical Co., Inc. Homemade deionized water (Millipore, Elix, USA, MA) was used throughout this study.

Preparation of $(CH_3NH_3)VO_3$: V_2O_5 (2.05 g, V: 22.5 mmol) was mixed with 5.4 mL of 40% methylamine solution with a methylamine/V ratio of 2.8. The resulting mixture was then stirred for 30 min forming in a colorless solution. The solution was heated at 70 °C under atmospheric pressure to remove the unreacted methylamine and water, and 3.04 g of a white solid was obtained. Thermogravimetric analysis (TGA) revealed a 30.6% weight loss upon heating at 400 °C, which corresponds to the loss of 1 CH_3NH_2 and 0.5 H_2O from $(CH_3NH_3)VO_3$ to form V_2O_5 (30.5%). IR, $\tilde{\nu}/cm^{-1}$(KBr): 3000 (m), 1614 (m), 1594 (sh), 1506 (m), 1490 (m), 1473 (w), 1457 (m), 1419 (w), 1263 (w), 939 (s, sh), 919 (vs), 894 (s), 831 (vs), 777 (vs), 655 (vs). Elemental analysis calcd. for $(CH_3NH_3)VO_3$: H 4.63, C 9.17, N 10.69; found, H 4.53, C 9.03, N 10.39.

Single crystals of $(CH_3NH_3)VO_3$: $(CH_3NH_3)VO_3$ (0.1 g) was dissolved in 1 mL of water at 60 °C and the temperature was slowly decreased to room temperature. Colorless crystals suitable for single-crystal X-ray structural analysis were obtained after 24 h.

Calcination of $(CH_3NH_3)VO_3$: $(CH_3NH_3)VO_3$ was calcined in air at 100, 125, 150, 175, 200, 225, 250, 275, 300, 325, and 350 °C. The temperature was increased to the target temperature at a heating rate of 10 °C/min and the temperature was maintained for 1 h.

Analytical techniques: Powder X-ray diffraction patterns were measured on a Bruker D2 PHASER 2nd Gen using Cu-K_α radiation. The samples were ground, placed on a sample holder, and the XRD profiles were recorded in the 2θ range of 3°–80°. Fourier transform infra-red (FT-IR) spectra were obtained on a NICOLET 6700 FT-IR spectrometer (Thermo Fischer Scientific) in the wavenumber range of 500–4000 cm^{-1} in KBr pellets. Thermogravimetric–differential thermal analysis (TG-DTA) was performed on a TG-DTA7300 instrument (SII) with an air or nitrogen flow of 200 mL s^{-1}. Temperature programmed desorption (TPD) was performed using a BELCAT II – BELMASS system (MicrotracBEL Corp.) under a flow of helium gas. The heating rate was 10 °C min^{-1} and the maximum temperature was 600 °C. ^{51}V NMR spectra were recorded using JEOL JNM-LA400 (V resonance frequency: 105.15 MHz) at 25 °C. The spectra were reference to the external $VOCl_3$ (0 ppm). Ultraviolet-visible spectra were obtained using an Agilent 8453 UV-visible spectrometer in the range of 190–1100 nm with a cell length of 1 cm. Raman spectra were collected using a JASCO RMP-510 with a 532.0 nm laser and each spectrum was collected for 1 s and accumulated three times. Differential scanning calorimetry (DSC) was performed using an EXSTAR DSC7020 instrument (Hitachi High-Tech Corp.) with a nitrogen flow rate of 50 mL s^{-1}. The temperature changing rate was 10 °C min^{-1} and the temperature range was 25 to −147 °C. CHN analyses were performed at Division of Instrumental Analysis, Okayama University.

X-ray crystallography: Single-crystal X-ray diffraction data for $(CH_3NH_3)VO_3$ were collected at 23, 0, −50, −100, and −150 °C on a Bruker SMART APEX2 instrument using Mo K_α radiation (λ = 0.71073 Å) monochromated by a layered confocal mirror. Data reduction and space group determination were performed using the Bruker APEX 3 suite.[55] Absorption correction was applied using a multi-scan technique (SADABS).[55] The structure was solved by direct methods using SHELXT[56] and refined using SHELXL[57] using the SHELXle[58] interface. We assigned N and C in one methylammonium cation ($CH_3NH_3^+$) by checking the distances between these atoms and the oxygen atoms bound to V. The crystal data obtained at 23 and −150 °C are summarized in Table 1 and Table S1.

Deposition Numbers 2158737 (for −150 °C), 2158738 (for 23 °C), 2169861 (for −100 °C), 2169862 (for −50 °C), and 2169863 (for 0 °C) contain the supplementary crystallographic data for this paper. These data are provided free of charge by the joint Cambridge Crystallographic Data Centre and Fachinformationszentrum Karlsruhe Access Structures service www.ccdc.cam.ac.uk/structures.

Preparation of SARS-CoV-2: VeroE6/TMPRSS2 cells [African green monkey kidney-derived cells expressing human TMPRSS2, purchased from Japanese Collection of Research Bioresources (JCRB) Cell Bank, JCRB1819] were propagated in Dulbecco's modified Eagle's minimum essential medium (DMEM; Invitrogen) supplemented with 10% fetal calf serum (FCS; Biosera, Kansas City, MO, U.S.A.), penicillin G (100 units/mL; Meiji Seika Pharma, Tokyo, Japan), and streptomycin (100 μg/mL; Meiji Seika Pharma). The cells were cultured at 37 °C in 5% CO_2. VeroE6/TMPRSS2 cells were infected with SARS-CoV-2/JP/HiroC77/2021 [Delta (B.1.617.2-like), EPI_ISL_6316561] at an input multiplicity of infection of 0.01. The infected cell culture medium was collected at 48 h post-infection, clarified using low-speed centrifugation, and filtered through a 0.45-μm filter. SARS-CoV-2 was further concentrated via ultracentrifugation at 22,000 rpm for 90 min using a 20% (w/w) sucrose/PBS cushion on a Beckman SW32 Ti rotor. The virus pellet was resuspended in 0.9% (w/v) NaCl for transmission electron microscopy (TEM) observation. Virus culture was performed at the P3 facility of Hiroshima University under Biosafety Level 3 regulations.

TEM observations: For TEM analysis, the virus solution (3 μL) was adsorbed onto a glow-discharged (PIB-10, VACUUM DEVICE PIB-10, Ibaraki, Japan) formvar and carbon-coated Cu grid (EM Japan, Tokyo, Japan) for 30 s. The excess solution was removed using filter paper. Subsequently, a drop (3 μL) of 0.9%(w/v) NaCl was placed in contact with the grid for 30 s for washing and blotted with filter paper. Finally, the staining solution (0.5 wt.% in water) was placed on the grid for 30 s and the excess solution was removed using filter paper. The staining step was performed twice and the grid was air-dried and irradiated with UV light (Care222™, Ushio Inc., Tokyo, Japan) to completely inactivate the virus.[59] The grid preparation was performed at the P3 facility of Hiroshima University under Biosafety Level 3 regulations. The sample grids were observed using TEM (JEOL, JEM-1400) with a tungsten filament operated at 80 kV at the Natural Science Center for Basic Research and Development, Hiroshima University. Images were recorded on a CCD camera (1024×1024 pixels).

Acknowledgements

This study was supported by JST A-STEP (Grant Number JPMJTM20RF), the International Network on Polyoxometalate Science at Hiroshima University, and the JSPS Core-to-Core program. N. C. S. would like to thank the financial support from the Osimo Scholarship and Program for Developing and Supporting the Next Generation of Innovative Researchers at Hiroshima University. The authors are grateful to Ms. M. Kosaka and Mr. M. Kobayashi at Division of Instrumental Analysis, Okayama University for the measurements of CHN elemental analyses, and Ms. K. Koike at Natural Science Center for Basic Research and Development, Hiroshima University for support to use TEM.

Conflict of Interest

The authors declare no conflict of interest.

Data Availability Statement

The data that support the findings of this study are available in the supplementary material of this article.

Keywords: Negative staining reagents · Polyoxometalates · Polyoxovanadates · Structure elucidation · Thermochemistry

[1] M. T. Pope, in *Heteropoly and Isopoly Oxometalates*, Springer-Verlag, Berlin, **1983**.
[2] C. L. Hill, *Chem. Rev.* **1998**, *98*, 1–2 (and articles within this special POM-themed issue).
[3] L. Cronin, A. Müller, *Chem. Soc. Rev.* **2012**, *41*, 7333–7334 (and articles within this special POM-themed issue).
[4] M. Ahmadian, M. Anbia, *Energy Fuels* **2021**, *35*, 10347–10373.
[5] S.-S. Wang, G.-Y. Yang, *Chem. Rev.* **2015**, *115*, 4893–4962.
[6] M. Sadakane, E. Steckhan, *Chem. Rev.* **1998**, *98*, 219–237.

[7] N. Li, J. Liu, B.-X. Dong, Y.-Q. Lan, *Angew. Chem. Int. Ed.* **2020**, *59*, 20779–20793; *Angew. Chem.* **2020**, *132*, 20963–20977.
[8] A. Bijelic, M. Aureliano, A. Rompel, *Angew. Chem. Int. Ed.* **2019**, *58*, 2980–2999; *Angew. Chem.* **2019**, *131*, 3008–3029.
[9] M. I. S. Veríssimo, D. V. Evtuguin, M. T. S. R. Gomes, *Front. Chem.* **2022**, *10*, 840657.
[10] C. A. Scarff, M. J. G. Fuller, R. F. Thompson, M. G. Iadanza, *J. Visualization* **2018**, *132*, e57199.
[11] K. Sahiro, Y. Kawato, K. Koike, T. Sano, T. Nakai, M. Sadakane, *Sci. Rep.* **2022**, *12*, 7554.
[12] N. I. Gumerova, A. Rompel, *Chem. Soc. Rev.* **2020**, *49*, 7568–7601.
[13] D.-L. Long, E. Burkholder, L. Cronin, *Chem. Soc. Rev.* **2007**, *36*, 105–121.
[14] K. Y. Monakhov, W. Bensch, P. Kögerler, *Chem. Soc. Rev.* **2015**, *44*, 8443–8483.
[15] J. Zhou, J.-W. Zhao, Q. Wei, J. Zhang, G.-Y. Yang, *J. Am. Chem. Soc.* **2014**, *136*, 5065–5071.
[16] Y. Hayashi, *Coord. Chem. Rev.* **2011**, *255*, 2270–2280.
[17] N. Wang, Z. He, M. Cui, W. Guo, S. Zhang, M. Yang, *Cryst. Growth Des.* **2015**, *15*, 1619–1624.
[18] E. E. Hamilton, P. E. Fanwick, J. J. Wilker, *J. Am. Chem. Soc.* **2002**, *124*, 78–82.
[19] J. Li, C. Wei, D. Guo, C. Wang, Y. Han, G. He, J. Zhang, X. Huang, C. Hu, *Dalton Trans.* **2020**, *49*, 14148–14157.
[20] V. W. Day, W. G. Klemperer, O. M. Yaghi, *J. Am. Chem. Soc.* **1989**, *111*, 4518–4519.
[21] I. Mestiri, I. Nagazi, A. Haddad, *J. Soc. Chim. Tunis.* **2015**, *17*, 128–134.
[22] Y. Kikukawa, K. Ogihara, Y. Hayashi, *Inorganics* **2015**, *3*, 295–308.
[23] A. Müller, E. Krickerneyer, M. Penk, H.-J. Walberg, H. Bögge, *Angew. Chem. Int. Ed.* **1987**, *26*, 1045–1046; *Angew. Chem.* **1987**, *99*, 1060–1061.
[24] K. Pavani, S. Upreti, A. Ramanan, *J. Chem. Sci.* **2006**, *118*, 159–164.
[25] J. Marrot, K. Barthelet, C. Simonnet, D. Riou, *C. R. Chim.* **2005**, *8*, 971–976.
[26] Y. Hayashi, K. Fukuyama, T. Takatera, A. Uehara, *Chem. Lett.* **2000**, *29*, 770–771.
[27] T. Yamase, M. Suzuki, K. Ohtaka, *J. Chem. Soc. Dalton Trans.* **1997**, 2463–2472.
[28] A. Müller, M. Penk, E. Krickemeyer, H. Bögge, H.-J. Walberg, *Angew. Chem. Int. Ed.* **1988**, *27*, 1719–1721; *Angew. Chem.* **1988**, *100*, 1787–1789.
[29] A. Müller, R. Rohlfing, J. Döring, M. Penk, *Angew. Chem. Int. Ed.* **1991**, *30*, 588–590; *Angew. Chem.* **1991**, *103*, 575–577.
[30] M. T. Averbuch-Pouchot, A. Durif, *C. R. Acad. Sci. Ser. II* **1994**, *318*, 1067–1072.
[31] A. Pérez-Benítez, S. Bernès, *IUCrData* **2018**, *3*, x181080.
[32] M. Aureliano, N. I. Gumerova, G. Sciortino, E. Garribba, A. Rompel, D. C. Crans, *Coord. Chem. Rev.* **2021**, *447*, 214143.
[33] D. Rehder, *Angew. Chem. Int. Ed.* **1991**, *30*, 148–167; *Angew. Chem.* **1991**, *103*, 152–172.
[34] D. Liu, Y. Lu, H.-Q. Tan, W.-L. Chen, Z.-M. Zhang, Y.-G. Li, E.-B. Wang, *Chem. Commun.* **2013**, *49*, 3673–3675.
[35] B. Franzetti, G. Schoehn, J.-F. Hernandez, M. Jaquinod, R. W. H. Ruigrok, G. Zaccai, *EMBO J.* **2002**, *21*, 2132–2138.
[36] J. Ma, L.-W. Wang, *Nano Lett.* **2015**, *15*, 248–253.
[37] A. A. Bakulin, O. Selig, H. J. Bakker, Y. L. A. Rezus, C. Müller, T. Glaser, R. Lovrincic, Z. Sun, Z. Chen, A. Walsh, J. M. Frost, T. L. C. Jansen, *J. Phys. Chem. Lett.* **2015**, *6*, 3663–3669.
[38] M. Aureliano, N. I. Gumerova, G. Sciortino, E. Garribba, C. C. McLauchlan, A. Rompel, D. C. Crans, *Coord. Chem. Rev.* **2022**, *454*, 214344.
[39] J. C. Pessoa, M. F. A. Santos, I. Correia, D. Sanna, G. Sciortino, E. Garribba, *Coord. Chem. Rev.* **2021**, *449*, 214192.
[40] A. Ścibior, *Antioxidants* **2022**, *11*, 790.
[41] P. Zhou, X.-L. Yang, X.-G. Wang, B. Hu, L. Zhang, W. Zhang, H.-R. Si, Y. Zhu, B. Li, C.-L. Huang, H.-D. Chen, J. Chen, Y. Luo, H. Guo, R.-D. Jiang, M.-Q. Liu, Y. Chen, X.-R. Shen, X. Wang, X.-S. Zheng, K. Zhao, Q.-J. Chen, F. Deng, L.-L. Liu, B. Yan, F.-X. Zhan, Y.-Y. Wang, G.-F. Xiao, Z.-L. Shi, *Nature* **2020**, *579*, 270–273.
[42] R. Lu, X. Zhao, J. Li, P. Niu, B. Yang, H. Wu, W. Wang, H. Song, B. Huang, N. Zhu, Y. Bi, X. Ma, F. Zhan, L. Wang, T. Hu, H. Zhou, Z. Hu, W. Zhou, L. Zhao, J. Chen, Y. Meng, J. Wang, Y. Lin, J. Yuan, Z. Xie, J. Ma, W. J. Liu, D. Wang, W. Xu, E. C. Holmes, G. F. Gao, G. Wu, W. Chen, W. Shi, W. Tan, *Lancet* **2020**, *395*, 565–574.
[43] W. Baschong, U. Aebi, in *Negative Staining. Cell Biology: A Laboratory Handbook, 3rd Ed, Vol. 3*, Academic Press, Cambridge, Massachusetts, **2006**.
[44] A. Takanabe, T. Katsufuji, K. Johmoto, H. Uekusa, M. Shiro, H. Koshima, T. Asahi, *Crystals* **2017**, *7*, 7.
[45] K. Wang, C. Wang, M. K. Mishra, V. G. Young Jr, C. C. Sun, *CrystEngComm* **2021**, *23*, 2648–2653.
[46] E. Tella, A. Trimpalis, A. Tsevis, C. Kordulis, A. Lycourghiotis, S. Boghosian, K. Bourikas, *Catalysts* **2021**, *11*, 322.
[47] A. M. Heyns, M. W. Venter, K.-J. Range, *Z. Naturforsch. B* **1987**, *42*, 843–852.
[48] N. Hu, J. Du, Y.-Y. Ma, W.-J. Cui, B.-R. Yu, Z.-G. Han, Y.-G. Li, *Appl. Surf. Sci.* **2021**, *540*, 148306.
[49] M. Iannuzzi, T. Young, G. S. Frankel, *J. Electrochem. Soc.* **2006**, *153*, B533–B541.
[50] E. Sánchez-Lara, S. Treviño, B. L. Sánchez-Gaytán, E. Sánchez-Mora, M. E. Castro, F. J. Meléndez-Bustamante, M. A. Méndez-Rojas, E. González-Vergara, *Front. Chem.* **2018**, *6*, 402.
[51] H. Ma, X. Meng, J. Sha, H. Pang, L. Wu, *Solid State Sci.* **2011**, *13*, 850–854.
[52] N. C. Sukmana, Sugiarto, Z. Zhang, M. Sadakane, *Z. Anorg. Allg. Chem.* **2021**, *647*, 1930–1937.
[53] D. M. Shayakhmetov, T. Papayannopoulou, G. Stamatoyannopoulos, A. Lieber, *J. Virol.* **2000**, *74*, 2567–2583.
[54] H. Yao, Y. Song, Y. Chen, N. Wu, J. Xu, C. Sun, J. Zhang, T. Weng, Z. Zhang, Z. Wu, L. Cheng, D. Shi, X. Lu, J. Lei, M. Crispin, Y. Shi, L. Li, S. Li, *Cell* **2020**, *183*, 730–738.
[55] Bruker, *APEX3*, *SADAB5*, *SAINT*, **2016**.
[56] G. M. Sheldrick, *Acta Crystallogr. Sect. A* **2008**, *64*, 112–122.
[57] G. M. Sheldrick, *Acta Crystallogr. Sect. C* **2015**, *71*, 3–8.
[58] C. B. Hübschle, G. M. Sheldrick, B. Dittrich, *J. Appl. Crystallogr.* **2011**, *44*, 1281–1284.
[59] H. Kitagawa, T. Nomura, T. Nazmul, K. Omori, N. Shigemoto, T. Sakaguchi, H. Ohge, *Am. J. Infect. Control* **2021**, *49*, 299–301.

Manuscript received: May 18, 2022
Revised manuscript received: July 1, 2022
Accepted manuscript online: July 4, 2022